Supplementary Information

# Achieving photostability in dye-sensitized upconverting nanoparticles and their use in Fenton type photocatalysis

Mannu Kaur, Steven L. Maurizio, Gabrielle A. Mandl, John A. Capobianco

## Table of Contents

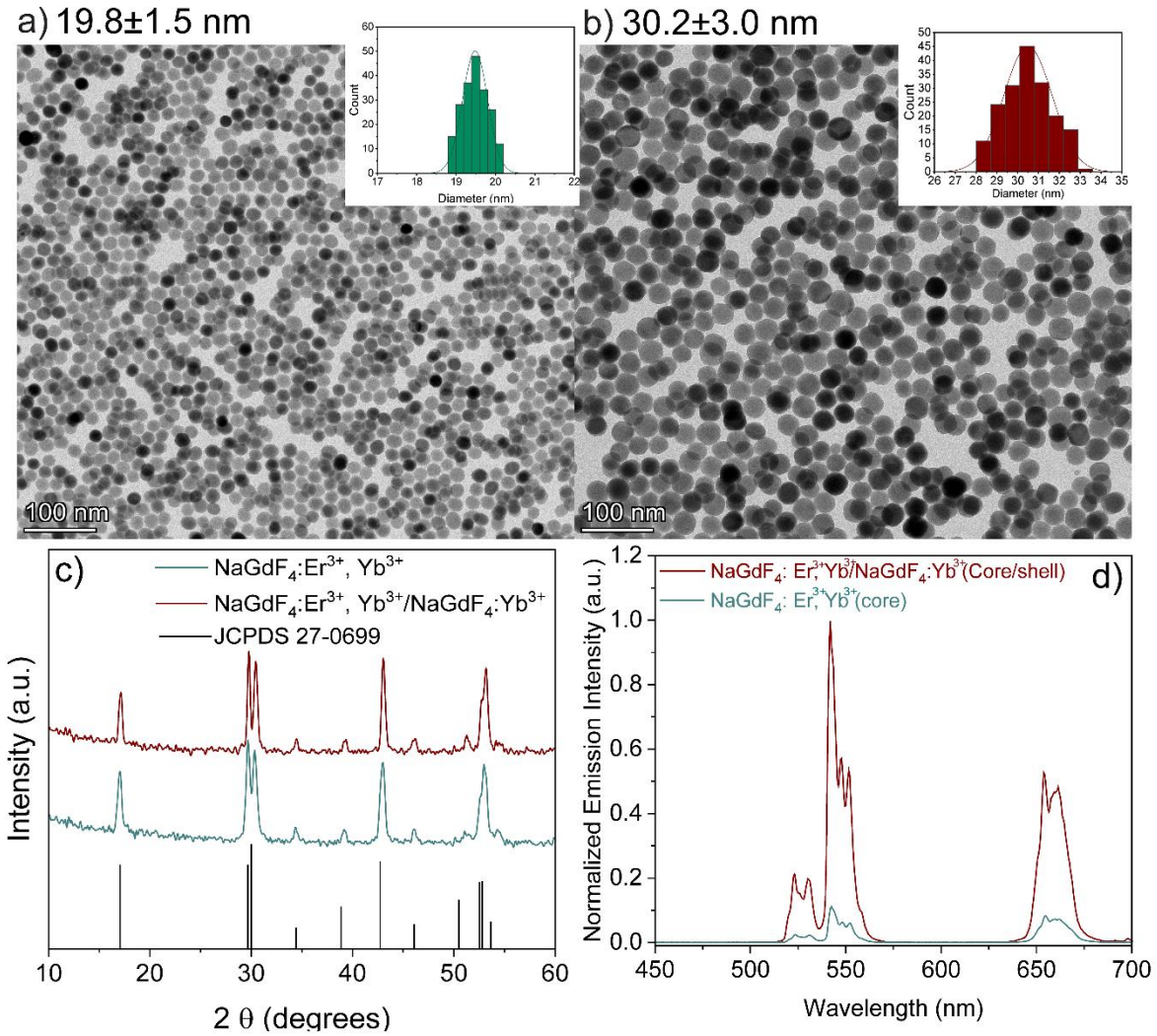


**Figure S1.** TEM micrographs of a) $NaGdF_4:Er^{3+}$, $Yb^{3+}$ (core nanoparticles) b) $NaGdF_4:Er^{3+}$, $Yb^{3+}$/ $NaGdF_4$: $Yb^{3+}$ (active core/active shell nanoparticles) with insets of their respective size distribution. c) Experimental XRD patterns of $NaGdF_4:Er^{3+}$, $Yb^{3+}$ (green) $NaGdF_4:Er^{3+}$, $Yb^{3+}$/ $NaGdF_4$: $Yb^{3+}$ (red) with a simulated line pattern for hexagonal phase $NaGdF_4$ (bottom plot) is shown for reference (black). d) Upconversion emission spectra of the 2 mg/ml $NaGdF_4:Er^{3+}$, $Yb^{3+}$ (green) and $NaGdF_4:Er^{3+}$, $Yb^{3+}$/ $NaGdF_4$: $Yb^{3+}$ (red) at 976 nm excitation.

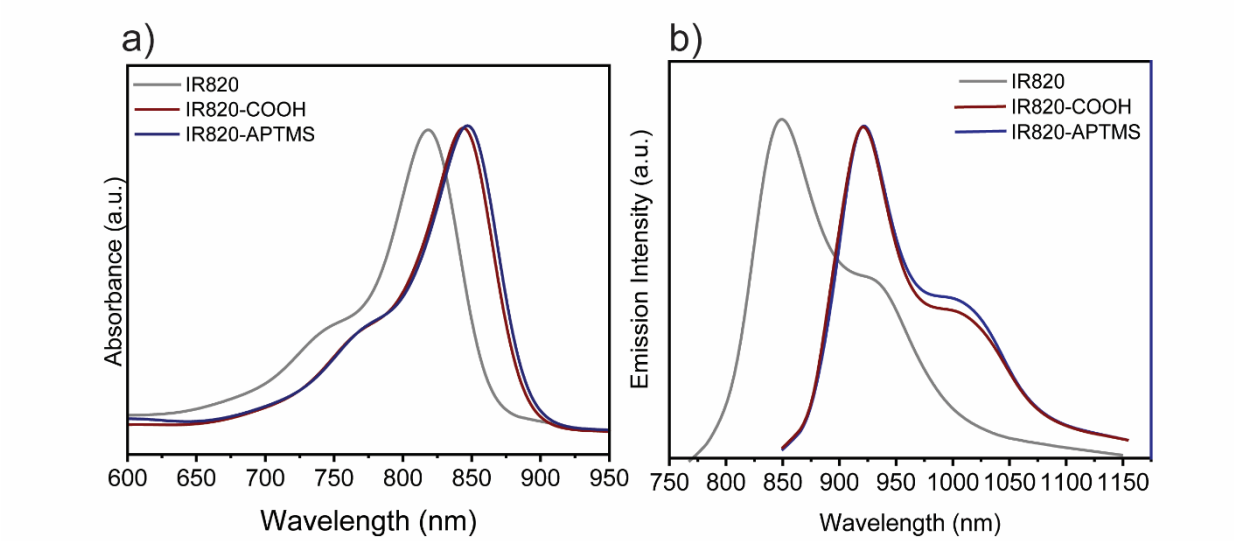


**Figure S2.** (a) Absorbance and (b) emission spectra of the synthesized IR820-COOH and IR820-APTMS, their comparison with IR820 dye (0.1 mg/ml in methanol).

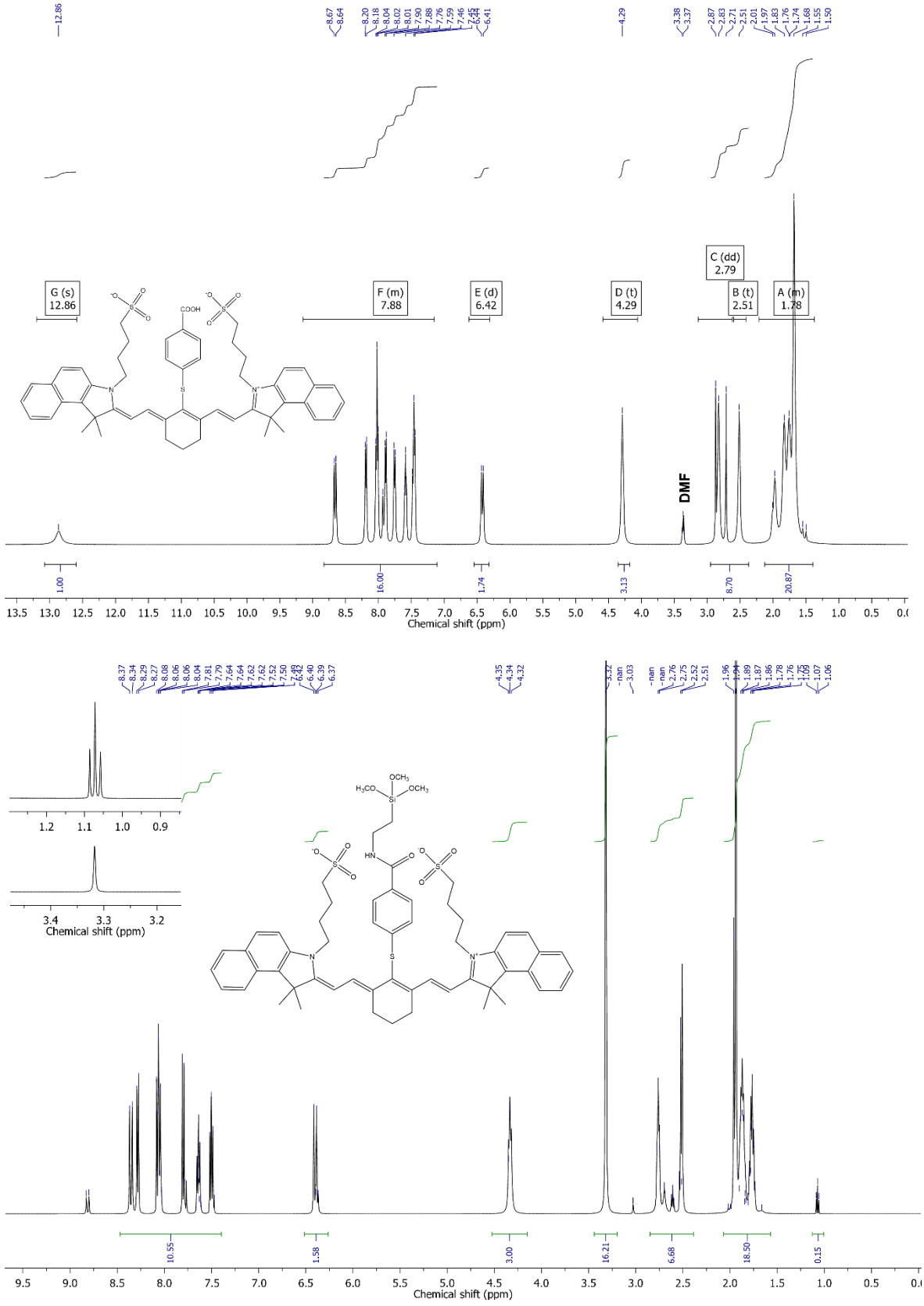


**Figure S3.** $^{1}$H NMR spectra of IR820-COOH (top) and IR820-APTMS (bottom) in DMSO-d6

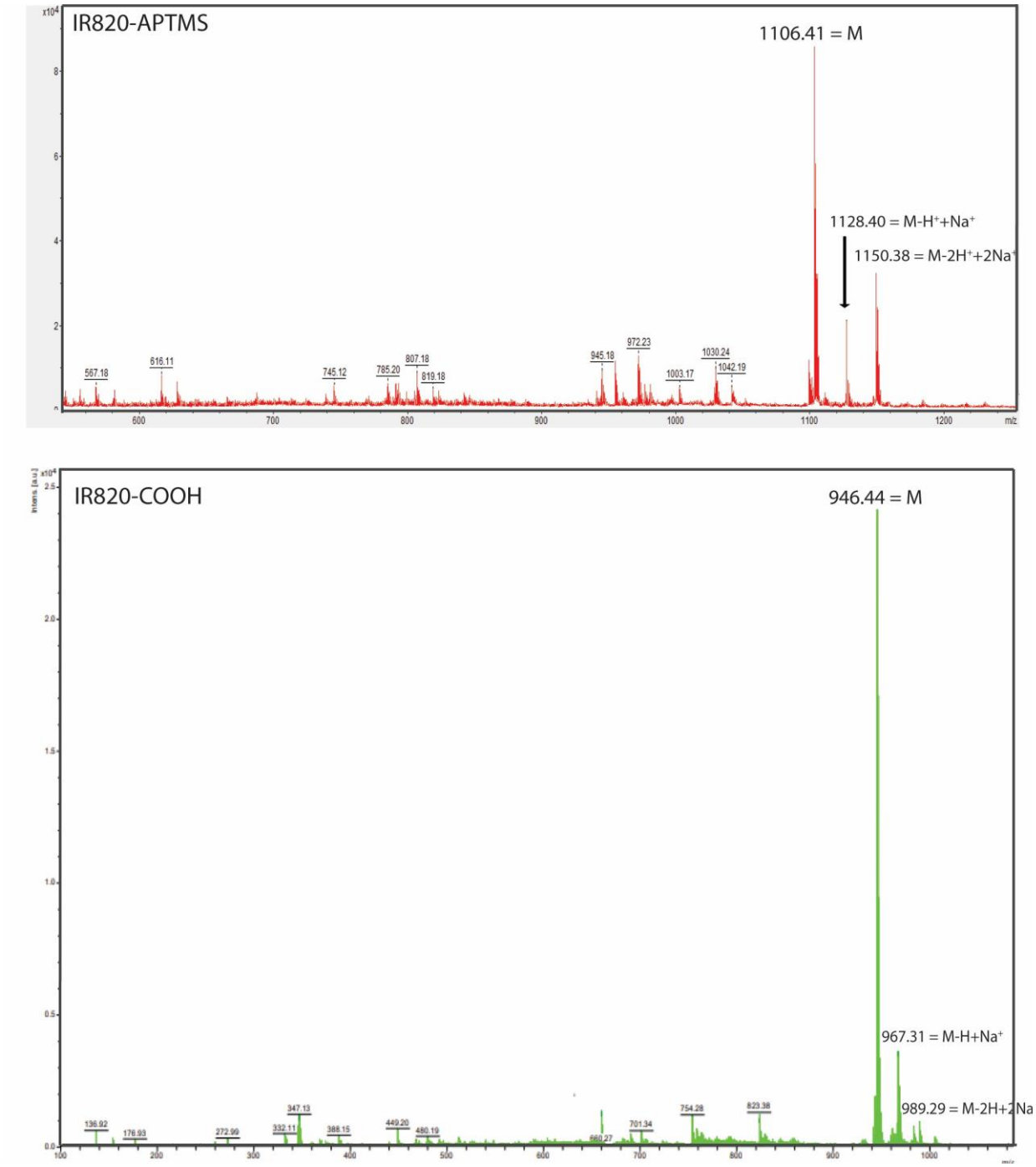


**Figure S4.** MALDI-TOF analysis of IR820-CONH-APTMS (MW=1106.41, top) and IR820-COOH (MW=946.44, bottom).

**Table S1**. Absorbance maximum, emission maximum, and molar extinction coefficients for IR820, IR820-COOH, and IR820-APTMS dyes in methanol

| NIR Dye | Absorbance maximum (nm) | Emission maximum (nm) | Extinction Coefficient ($M^{-1}cm^{-1}$) |
|---|---|---|---|
| IR820 | 820 | 850 | 198181.12 |
| IR820-COOH | 845 | 920 | 175625.58 |
| IR820-CONH-APTMS | 848 | 922 | 152256.89 |

**Table S2.** Moles of IR820-COOH dye, EDC and NHS were added to link different numbers of dye molecules in the SL system.

| IR820-COOH (nmol) | EDC (nmol) | NHS (nmol) |
|---|---|---|
| 10 | 10 | 25 |
| 20 | 20 | 50 |
| 28 | 28 | 70 |
| 34 | 34 | 85 |
| 42 | 42 | 105 |

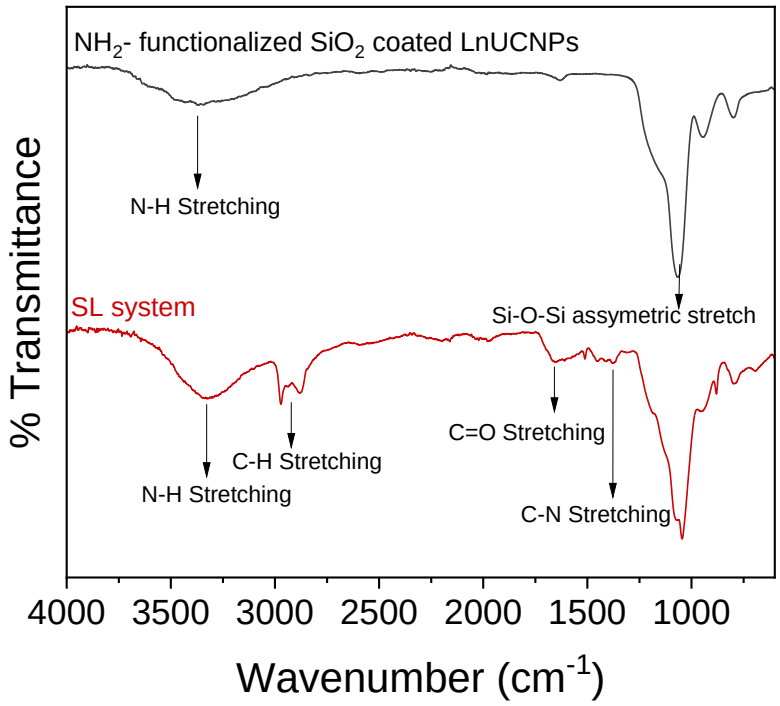


**Figure S5.** FTIR of $NH_2$ functionalized silica coated active-core/active-shell NPs (black) and IR820-COOH linked with amide coupling on the surface of the silica coated active-core/active-shell NPs (red).

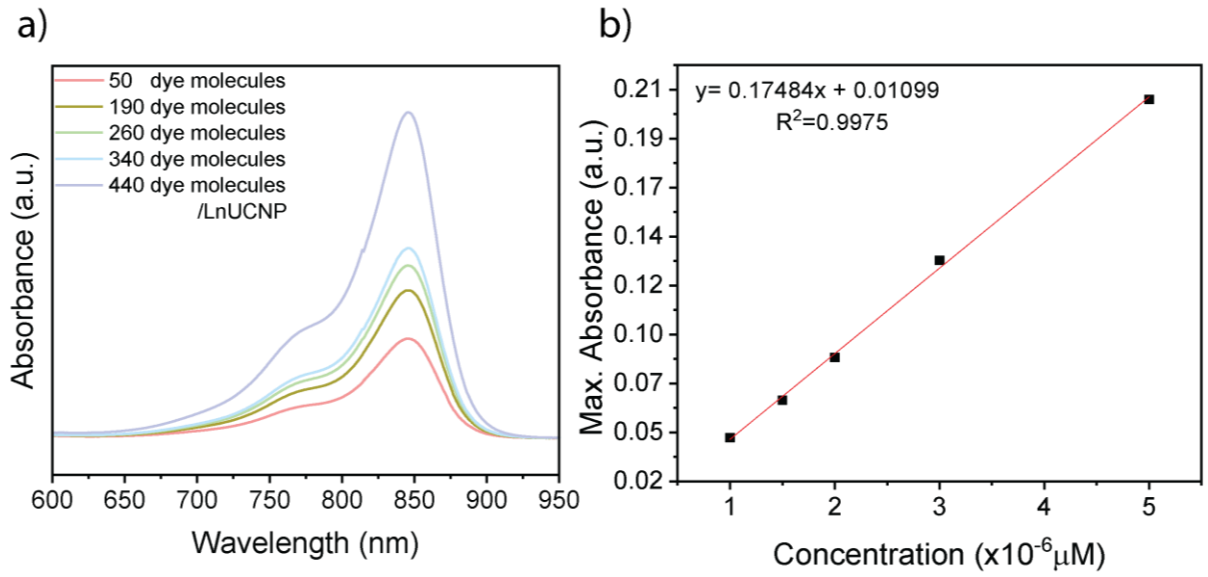


**Figure S6**. (a) UV-Vis absorption spectra for IR820-COOH dye molecules linked in SL system (b) UV-vis calibration curve to quantify the number of dye molecules

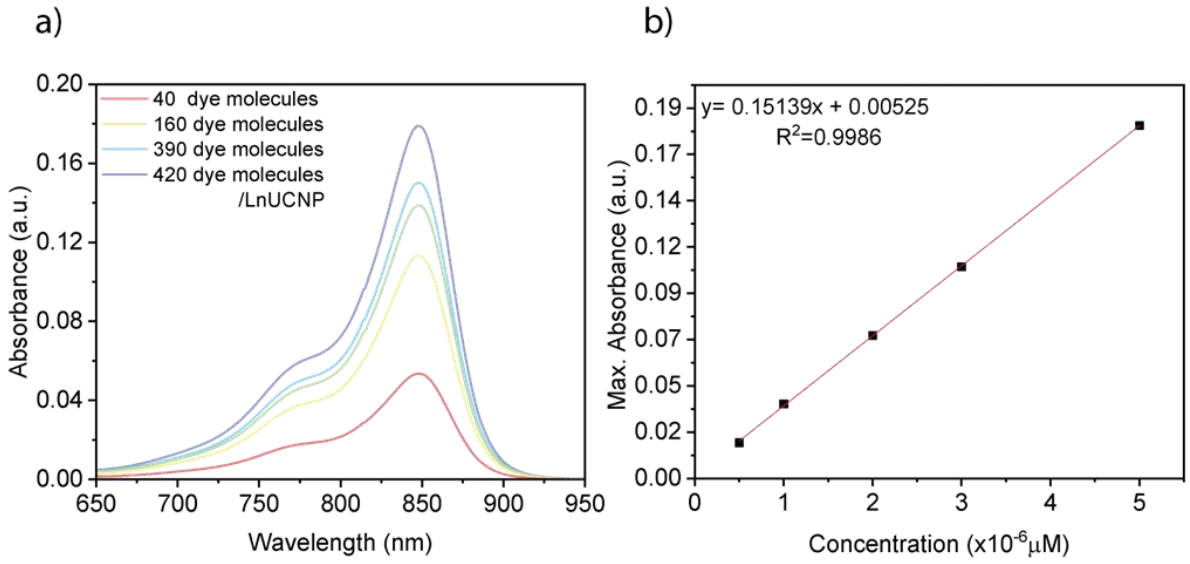


**Figure S7**. (a) UV-Vis absorption spectra for IR820-APTMS dye molecules embedded in SE system (b) UV-vis calibration curve to quantify the number of dye molecules

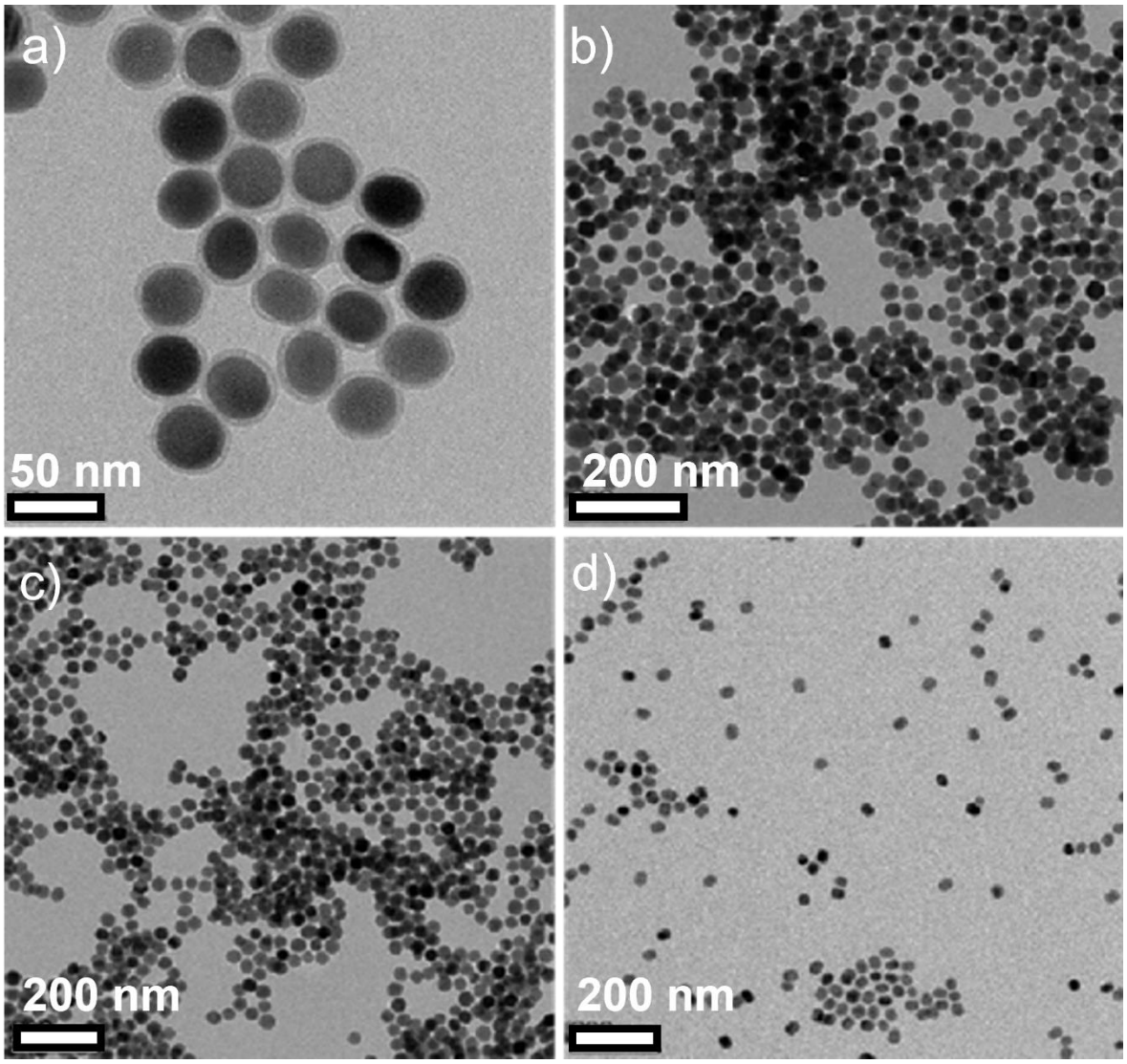


**Figure S8**. TEM micrograph of SE systems having varied amounts of dye embedded in the silica matrix with a thickness of a) 4 nmol dye, 4.2±1.2 nm b) 12 nmol dye, 4.0±0.7 nm c) 16 nmol dye, 4.5±1.5 nm d) 25 nmol dye, 5.2±1.0 nm. Amounts of dye correspond to those in Table S2.

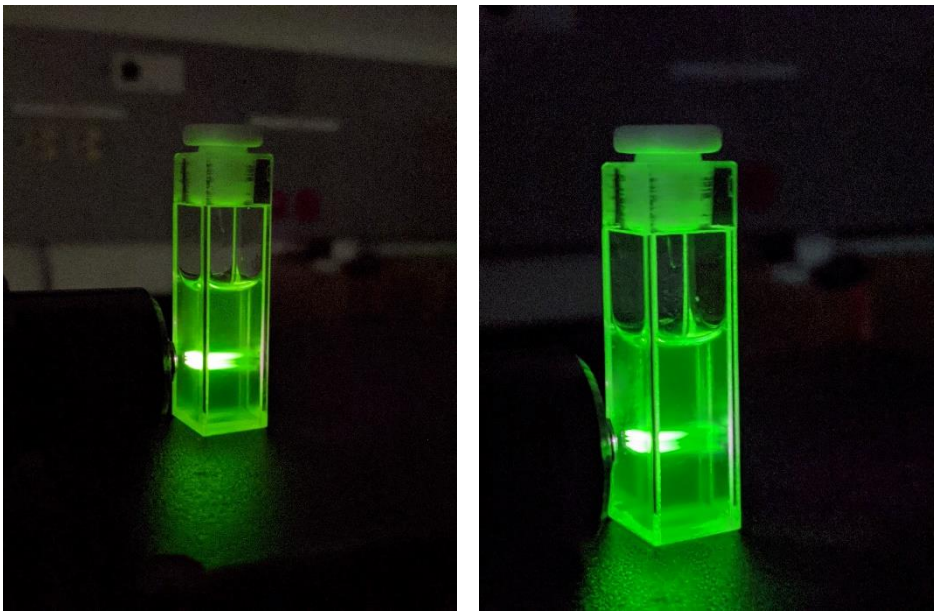

**Figure S9**. Photographs of 5 mg/mL solution in methanol of the (left) SL system and (right) SE system, under 808 nm irradiation.

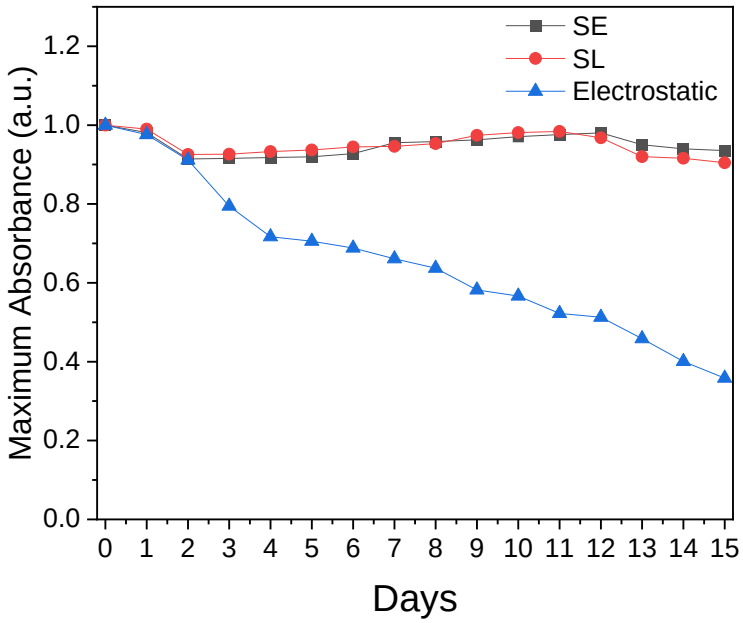


**Figure S10.** Absorbance as a function of incubation time for SE (black), SL (red) and electrostatic (blue) system to monitor leaking of dye from the nanoparticle surface. All samples are 5 mg/mL nanoparticles in methanol.

**Table S3.** Moles of IR820-CONH-APTMS dye and TEOS added to embed different numbers of dye molecules in the SE system.

| **IR820-CONH-APTMS (nmol)** | **TEOS (µmol)** |
|---|---|
| 4 | 26 |
| 12 | 18 |
| 16 | 14 |
| 20 | 10 |
| 25 | 5 |

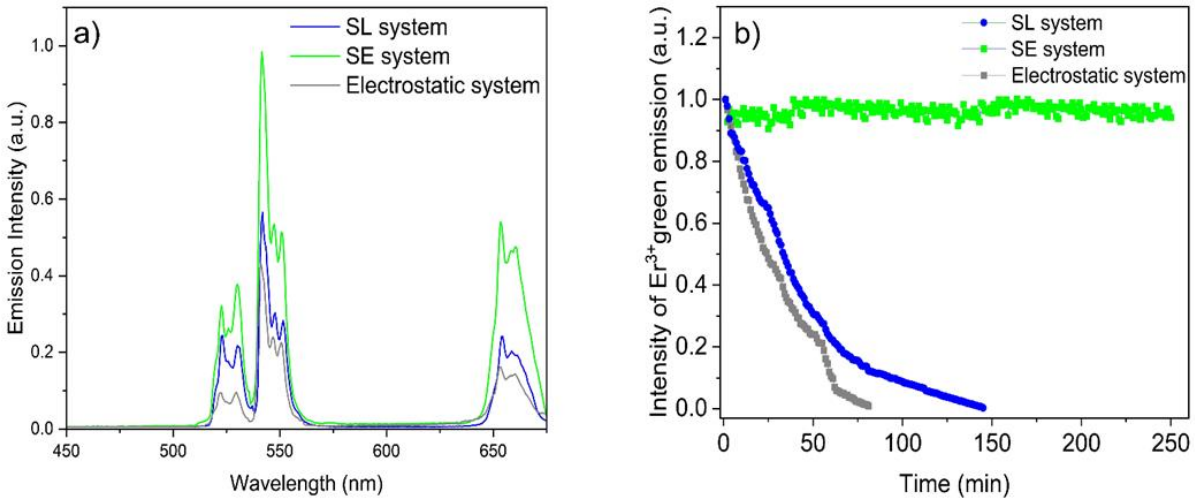


**Figure S11.** a) Comparison of UCL spectra of SL (green) SE (blue) and the electrostatic system (grey) with the dye coordinated to the oleate-free nanoparticle surface upon 808 nm excitation b) Overall emission intensities of SL (green), SE (blue) and electrostatic system (grey) as a function of irradiation time upon 808 nm excitation.

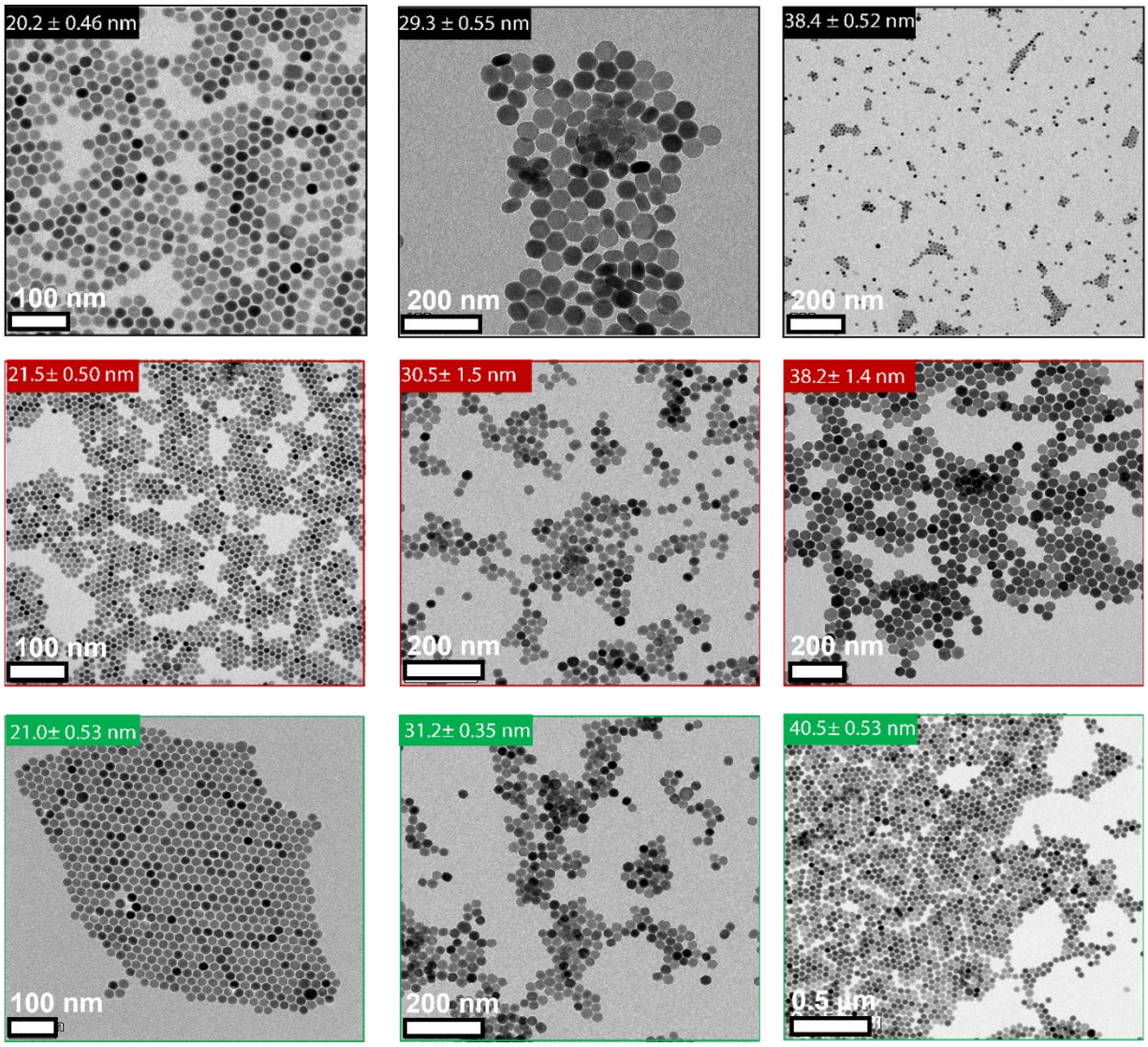


**Figure S12**. TEM micrographs of core, core/shell and core/shell/shell respectively for (a) $NaGdF_4:Er^{3+}$, $Yb^{3+}/NaGdF_4:Yb^{3+}/$ $NaGdF_4:10\%Nd^{3+}$ (black), $NaGdF_4:Er^{3+}$, $Yb/NaGdF_4:Yb^{3+}/$ $NaGdF_4:15\%Nd^{3+}$ (red), $NaGdF_4:Er,\ ^{3+}\ Yb^{3+}/NaGdF_4:Yb^{3+}/$ $NaGdF_4:20\%Nd^{3+}$ (green).

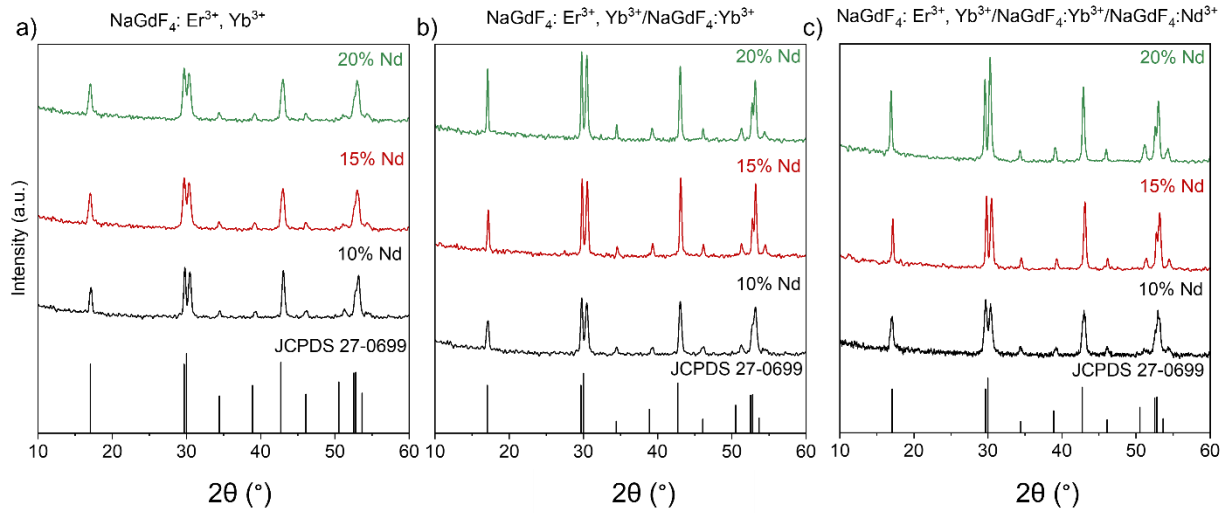


**Figure S13.** XRD patterns of (a) $NaGdF_4:Er^{3+}$, $Yb^{3+}$ (cores), (b) $NaGdF_4:Er^{3+}$, $Yb^{3+}$/ $NaGdF_4$: $Yb^{3+}$ (core/shell), (c) $NaGdF_4:Er^{3+}$, $Yb^{3+}$/ $NaGdF_4$: $Yb^{3+}$/ $NaGdF_4$: x%$Nd^{3+}$ (core/shell/shell), for 10% (black), 15% (red), 20% (green) $Nd^{3+}$-doped batches.

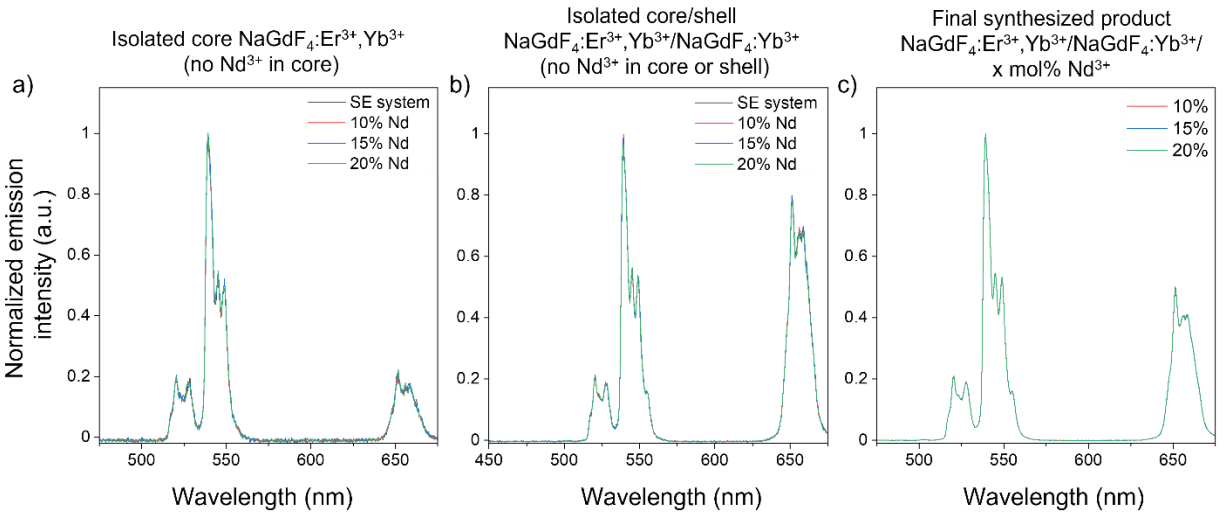


**Figure S14.** UCL spectra under 976 nm excitation of the (a) core and (b) core/shell nanoparticles isolated during the synthesis of (c) core/shell/shell LnUCNPs having 10 (red traces), 15 (blue traces) or 20 (green traces) mol% $Nd^{3+}$ in the outer shell or the core and core/shell samples taken during the synthesis of the SE system (black). An aliquot of the cores and core/shells during the synthesis of the final product was taken and purified to obtain these spectra at 2 mg/mL nanoparticles dispersed in hexanes.

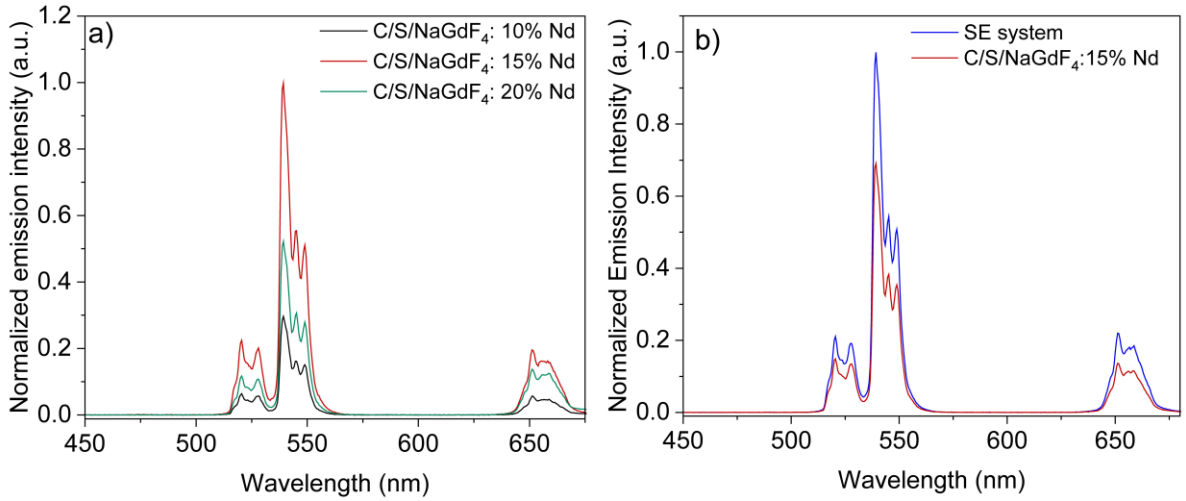


**Figure S15.** Normalized UCL spectra under 808 nm excitation for a) (core/shell/shell) $NaGdF_4:Er^{3+},Yb^{3+}/NaGdF_4:Yb^{3+}/NaGdF_4$: x%$Nd^{3+}$ x = 10, 15 or 20 mol% $Nd^{3+}$ concentrations (hexanes, 2 mg/mL dispersions) b) UCL spectra of oleate-free $NaGdF_4:Er^{3+},Yb^{3+}/NaGdF_4:Yb^{3+}/NaGdF_4$: 15% $Nd^{3+}$ and the SE system (2 mg/mL dispersions in methanol)

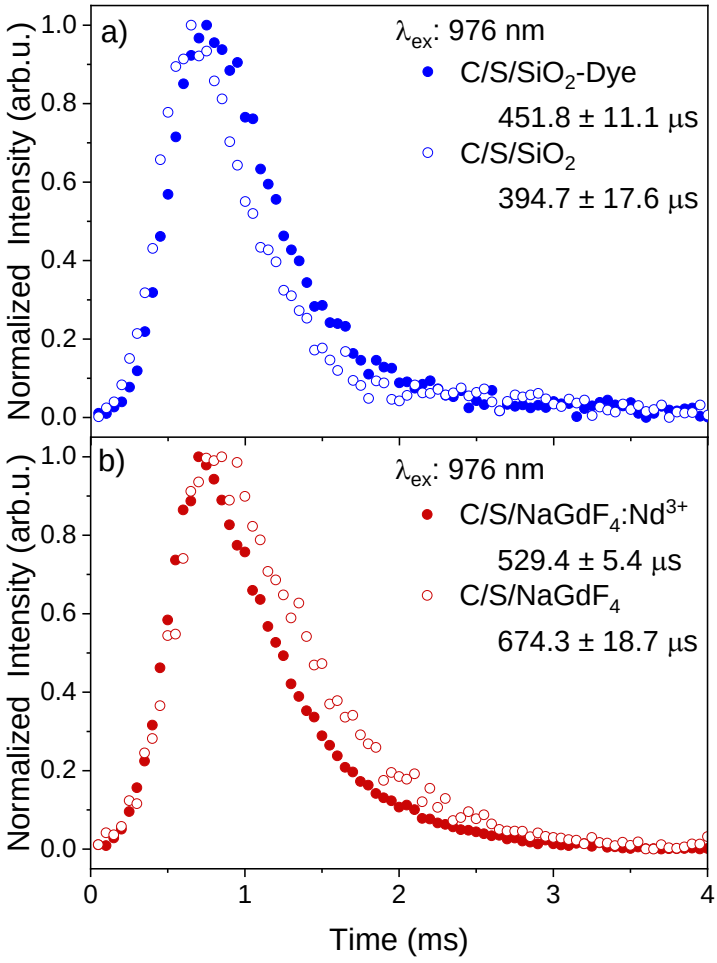


**Figure S16.** Upconversion lifetimes of the $^4F_{9/2} \rightarrow {}^4I_{15/2}$ transition of $Er^{3+}$ in (a) the SE system ($C/S/SiO_2$-Dye, filled) and $NaGdF_4:Yb^{3+},Er^{3+}/NaGdF_4:Yb^{3+}$ LnUCNPs coated with unfunctionalized silica ($C/S/SiO_2$, outlined) under 808 nm excitation. (b) $NaGdF_4:Yb^{3+},Er^{3+}/NaGdF_4:Yb^{3+}/NaGdF_4$:15% $Nd^{3+}$ LnUCNPs ($C/S/NaGdF_4:Nd^{3+}$, filled circles) and $NaGdF_4:Yb^{3+},Er^{3+}/NaGdF_4:Yb^{3+}/NaGdF_4$ LnUCNPs ($C/S/NaGdF_4$, outlined circles) under 976 nm excitation.

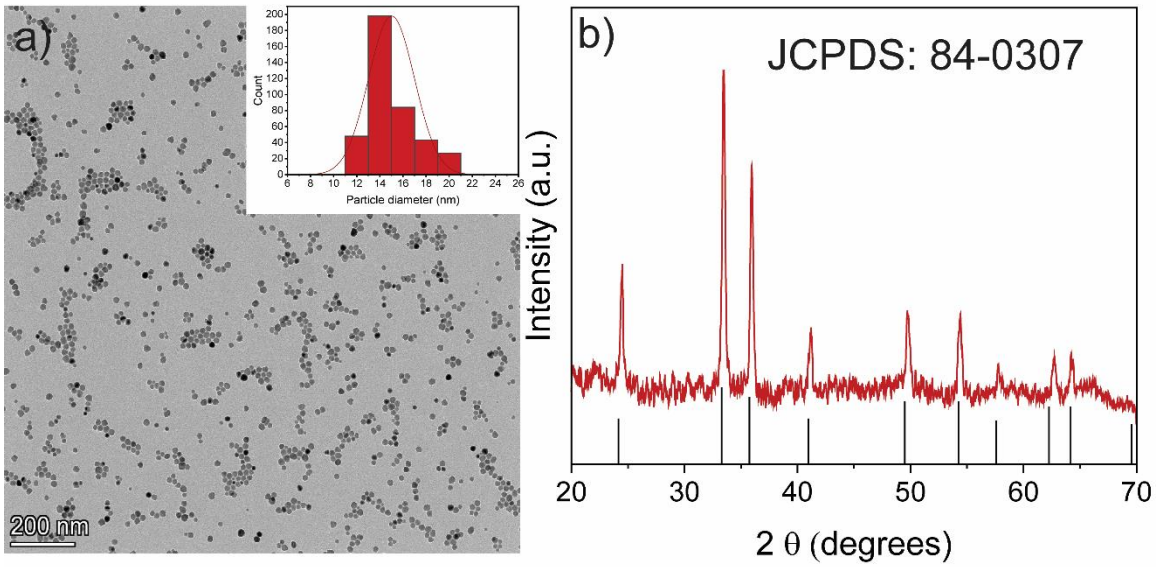


**Figure S17.** (a) TEM micrograph with the corresponding inset of the size distribution (15.5 ± 5.7 nm), (b) Experimental XRD (red) and JCPDS 84-0307 reference pattern (black) of hematite (α-$Fe_2O_3$) nanoparticles.

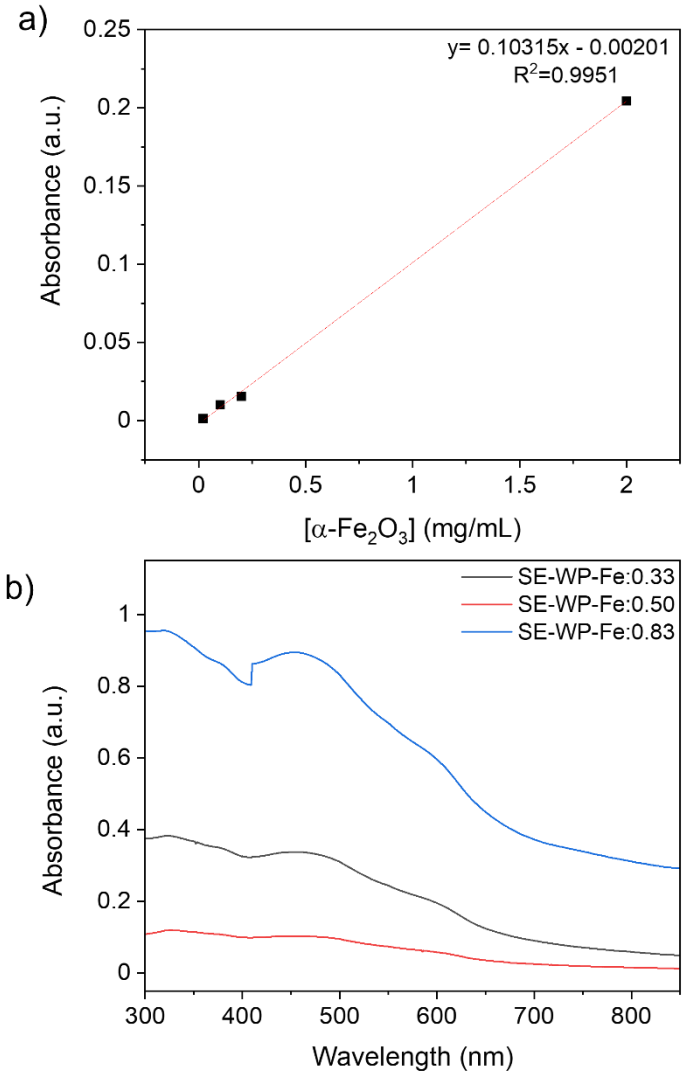


**Figure S18.** (a) Calibration curve generated from absorption spectra of dispersions of hematite nanoparticles in ethanol. (b) Absorbance spectrum both used for quantification of the hematite nanoparticles inserted into the pores of the SE-WP nanoparticles (2 mg/mL in methanol).

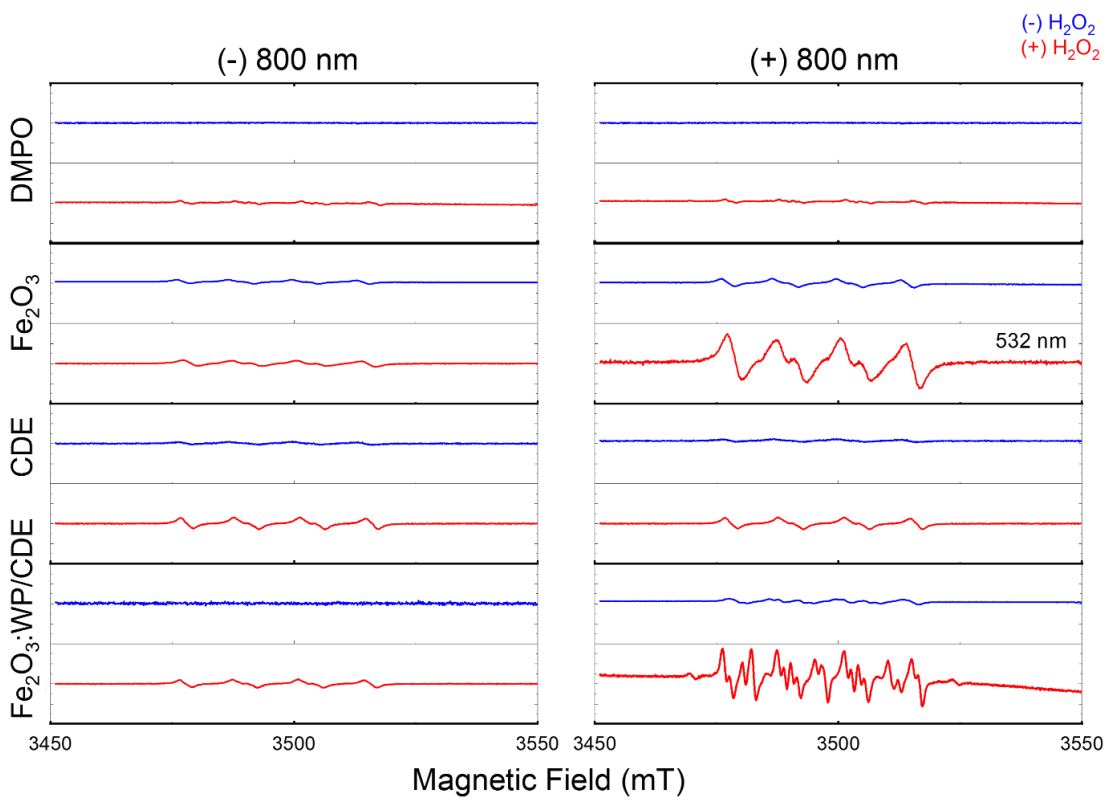


**Figure S19.** Electron paramagnetic resonance spectra of the SE-WP-Fe, SE, $Fe_2O_3$ with and without $H_2O_2$ (red and blue, respectively) with DMPO spin trapping agent with and without 800 nm excitation. All spectra were recorded using 2 mg/mL nanoparticles in methanol.

**Table S4.** Electron paramagnetic resonance (EPR) data corresponding to the spectra presented in Figure S19. All samples were recorded in methanol (2 mg/mL dispersions) at room temperature.

| Sample | $H_2O_2$ | 808 nm | aN | aH | aH2 | aN/aH | Assignment[1] |
|---|---|---|---|---|---|---|---|
| DMPO | (-) | (-) | -- | -- | -- | | N/A |
| DMPO | (+) | (-) | -- | -- | -- | | N/A |
| DMPO | (-) | (+) | -- | -- | -- | | N/A |
| DMPO | (+) | (+) | 13.8 | 11.1 | 1.2 | 1.24 | DMPO-OOH (superoxide) |
| $Fe_2O_3$ | (-) | 532 nm | 13 | 12.2 | -- | 1.09 | DMPO-X (degradation) |
| $Fe_2O_3$ | (-) | (-) | 13.1 | 10.3 | -- | 1.27 | DMPO-OH |
| $Fe_2O_3$ | (+) | (-) | -- | -- | -- | | |
| $Fe_2O_3$ | (-) | (+) | 13.1 | 10.3 | -- | 1.27 | DMPO-OH |
| $Fe_2O_3$ | (+) | (+) | 13.3 | 9.9 | -- | 1.34 | |
| SE system | (-) | (-) | -- | -- | -- | | |
| SE system | (+) | (-) | 13.5 | 10.9 | -- | 1.23 | DMPO-OOH (superoxide |
| SE system | (-) | (+) | -- | -- | -- | | |
| SE system | (+) | (+) | 13.5 | 10.9 | | 1.23 | DMPO-OOH (superoxide) |
| SE-WP-Fe 0.50 | (-) | (-) | -- | -- | -- | | -- |
| SE-WP-Fe 0.50 | (+) | (-) | -- | -- | -- | | -- |
| SE-WP-Fe 0.50 | (-) | (+) | 13.7 | 9.8 | 0.7 | 1.39 | DMPO-OH |
| SE-WP-Fe 0.50 | (-) | (+) | 13.9 | 6.7 | -- | 2.07 | DMPO-$CH_3O$ |
| SE-WP-Fe 0.50 | (-) | (+) | 12.9 | 9.75 | -- | 1.32 | DMPO-OH |
| SE-WP-Fe 0.50 | (+) | (+) | 13.8 | 11.2 | 1.2 | 1.23 | DMPO-OOH |
| SE-WP-Fe 0.50 | (+) | (+) | 12.9 | 9.9 | -- | 1.30 | DMPO-OH |
| SE-WP-Fe 0.50 | (+) | (+) | 13.9 | 14.6 | -- | 0.95 | DMPO-X (degradation) |

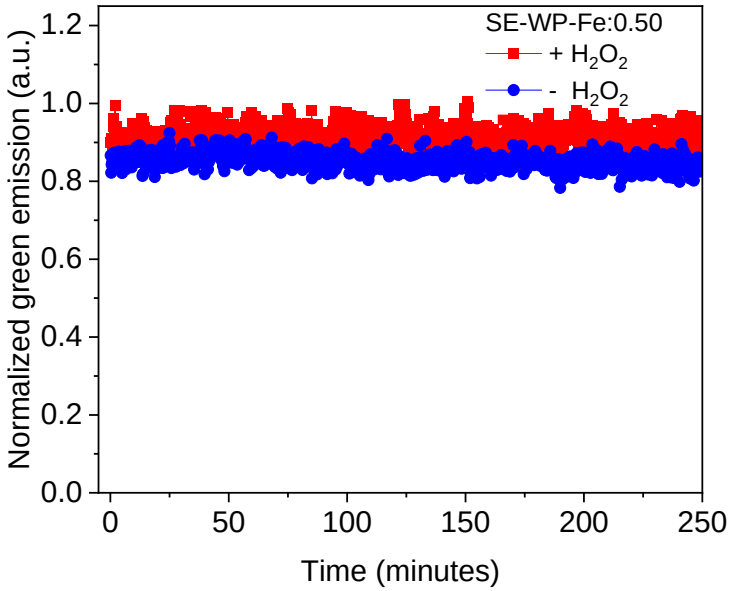


**Figure S20.** Emission intensity of the $^{2}H_{11/2} \rightarrow {}^{4}I_{15/2}$ transition of $Er^{3+}$ in the SE-WP-Fe:0.50 system (2 mg/mL dispersion in methanol) as a function of irradiation time (800 nm excitation) in the presence and absence of $H_2O_2$.

**References**

1 G. R. Buettner, *Free. Radic. Biol. Med.*, 1987, 3, 259–303.